DECEMBER 1983 LRP 232/83

RECENT ALFVEN WAVE HEATING RESULTS ON THE TCA TOKAMAK

R. Behn, A. de Chambrier, G.A. Collins, P.-A. Duperrex
A. Heym, F. Hofmann, Ch. Hollenstein, B. Joye,
R. Keller, A. Lietti, J.B. Lister, J.-M. Moret,
S. Nowak, J. O'Rourke, A. Pochelon and W. Simm

Invited Paper presented by J.B. Lister to the XI European Conference on Controlled Fusion and Plasma Physics, Aachan, September 1983

RECENT ALFVEN WAVE HEATING RESULTS ON THE TCA TOKAMAK

R. Behn, A. de Chambrier, G.A. Collins, P.-A. Duperrex, A. Heym, F. Hofmann, Ch. Hollenstein, B. Joye, R. Keller, A. Lietti, J.B. Lister, J.-M. Moret, S. Nowak[+], J. O'Rourke, A. Pochelon and W. Simm

Centre de Recherches en Physique des Plasmas
Association Euratom - Confédération Suisse
Ecole Polytechnique Fédérale de Lausanne
21, Av. des Bains, CH-1007 Lausanne/Switzerland

+Université de Fribourg, CH-1700 Fribourg/Switzerland

ABSTRACT

In this paper, we present the most recent results obtained during the Alfvén Wave Heating experiments being carried out on the TCA Tokamak. We have obtained both significant electron heating and some ion heating using rf powers up to 230 kW, greater than the value of the ohmic heating power in the target plasma. Firstly, we shall describe the AWH method as applied to TCA and then briefly cover some of the low power experiments carried out during the last year. The higher power experiments will then be discussed, along with some of the problems we have encountered.

INTRODUCTION

Alfvén Wave Heating generally refers to the resonant absorption of a wave's energy at a particular layer in a non-uniform plasma where the imposed wave's phase-velocity equals the local value of the Alfvén velocity. The Shear Alfvén resonance (sometimes referred to as the perpendicular ion-cyclotron resonance) is the major absorption mechanism available at frequencies below the ion cyclotron frequency, ω_{ci}. In common with other examples of resonant absorption, it has the property that the rate of transfer of energy is independent of the

actual dissipative processes. This frees us from the concern of how the energy is being dissipated, and leaves us to study the problem of coupling rf energy to the resonance layer.

Antennae external to the plasma create magnetic field and hence pressure modulations which are arranged to have both a definite frequency and definite wavelength. Theory and experiment have both demonstrated an improved loading of the antenna structure when it excites the so-called "surface wave". This is the first radial eigenmode of the asymmetrical ($m \neq 0$) fast wave in a plasma column surrounded by a vacuum layer, and is heavily damped at the Alfvén resonance layer.

Early experiments (namely in stellarators) used helical antennae, measuredthe antenna circuit loading and observed both heating and, in some cases, enhanced transport. At present, there are five experiments attacking AWH, some of which have changed to more convenient launching structures; they are Pretext (Bengtson et al., 1983), Tokapole II (Prager et al., 1983), Tortus (Cross et al., 1982), RO-5 (Demirkhanov et al., 1982) and TCA.

The TCA Tokamak has been described in detail elsewhere (Cheetham et al., 1980) and has major and minor radii of 61.5 and 18 cm respectively, $B_\phi \sim 11.6$ and 15.1 kG. The following results were obtained in a variety of conditions using hydrogen and deuterium as filling gases.

The antenna system comprises eight groups of three stainless steel antennae plates, phased in such a way as to excite the mode structure desired, usually N = 2, M = 1. The antennae are wide, and represent 16% of the plasma surface area. Experiments have been carried out at frequencies between 1.9 - 5.0 MHz with the high power work at 2.5 -2.6 MHz. This corresponds to a value of $\omega/\omega_{ci} \sim 0.23$ at 15 kG in deuterium. We note in passing that the range of ω/ω_{ci} covered by TCA (.2 - .8) overlaps the early operational range of JET, at 25 MHz in hydrogen for which $\omega/\omega_{ci} \sim 0.58$.

WAVE STUDIES

Our first low power experiments on TCA (de Chambrier et al., 1982a) confirmed the parametric dependence of the loading predicted by MHD theory, but surprisingly also revealed narrow resonances. These appeared as peaks in the loading at frequencies just below the start of the continua associated with the Alfvén resonance layers. These resonances have been identified as global eigenmodes of the Alfvén wave, which, although they do not exist for a non-uniform currentless plasma in ideal MHD theory, have been known to exist for many years as the result of the Hall term (ω/ω_{ci}). It has since been shown that the existence of magnetic field curvature (as a result of the plasma current) not only enhances the loading in the Alfvén continuum, but also enhances the excitation of these eigenmodes (Appert et al., 1982). The basic lack of coupling between different layers of the plasma for the Shear Alfvén Wave (Hasegawa and Uberoi, 1982) is removed by the effects of both finite frequency and field curvature, allowing the existence of global eigenmodes.

Experimentally we observed (and now it has been demonstrated theoretically) that these eigenmodes (or Discrete Alfvén Waves) only occur for one sign of helicity. That is, if the wave field is written in the cylindrical approximation as

$$b = b(r)e^{i(n\phi + m\theta - \omega t)} \qquad (1)$$

then DAWs only occur if n and m are of the same sign. Unlike the continuum loading, their usefulness for heating depends on the damping mechanism, and, like the fast wave eigenmodes, they suffer from being natural modes of the plasma, with large wave amplitudes.

We have continued low power experiments to study the spectrum of DAWs, observing eigenmodes with n ranging from 0 to 6, and have used magnetic pick-up probes to determine mode numbers and also to investigate the interference between the eigenmodes and the continua which have different n and m numbers. Of particular interest, both for DAWs and continuum loading, is the comparison with recent theoretical work

predicting a preference in the loading for modes with m negative. Our magnetic probe measurements have confirmed this theoretical result, the experiment being extremely clean due to our ability to select fairly pure mixtures of toroidal mode numbers in the excited waves, and also by the possibility of launching waves with a preferred toroidal direction. This latter work has confirmed the DAWs to be dominantly excited in the direction of electron drift, i.e. with both m and n negative, a result which may have a possible implication for current drive.

We show in Fig. 1 the measured antenna loading as a function of the plasma density (at constant frequency) with the antennae phased for N = 2, M = 1 excitation. This is compared with a cylindrical calculation which considers the contributions of the waves excited by the dominant Fourier components of the actual antenna current distributions. We can see in the Figure how the loading is made up from the various continua and discrete resonances. Considering the possible effects of toroidicity and surface dissipation as well as the use in the calculations of constant radial profiles and an artificial damping, the agreement of the general form of the loading is quite satisfactory. Up to the highest powers used, the loading resistance remains constant, suggesting that glow and arcing problems are not important at these levels.

HIGH POWER STUDIES

The heating experiments were carried out mainly in deuterium at 15.1 kG with I_p = 122 kA ($q_I \sim 3.3$) and I_p = 93 kA ($q_I \sim 4.3$). The driving frequency was 2.5 MHz and most results were obtained with an N = 2, M = 1 excitation structure. We have succeeded in delivering up to 170 kW averaged over the 30 msec rf pulse without causing a disruption, with maximum instantaneous power reaching 206 kW. We have exceeded the ohmic heating power before the rf pulse is applied at q_I = 4.3, P_{oh} = 142 kW, and almost equalled it at q = 3.3, P_{oh} = 215 kW. Power up to 220 kW has been delivered for up to 10 msec. Most of our work concentrated on discharges in which the sawtooth activity was not interrupted during the full rf pulse but we

shall later discuss the change in discharge character produced by the rf pulses. We note that the rf powers quoted are total electrical power lost from the antenna circuit due to the presence of the plasma. This quantity can be accurately measured during the rf pulse at this low frequency, since the resistive losses in the antenna circuit are known directly from the measured antenna current and calibrated resistance.

Previously (de Chambrier et al., 1982b) we had observed ion heating and electron heating, but the latter was confused due to apparent changes in profiles and in the transient nature of the temperature rise at higher power. We have now been able to confirm these, obtaining significant electron heating. In Fig. 2 we show the waveforms for a discharge with ~130 kW of rf power input. The plasma density, $n_e \sim 3\text{-}5 \times 10^{13} cm^{-3}$ during the rf pulse, puts us into the (n,m)=(2,-1) continuum, which has its resonant surface at r ~9-13 cm, and below the (n,m) = (-2,-1) DAW into which we cross at the highest powers.

Active control of the plasma density and current has given us a longer useful flat-top as well as maintenance of the q-value throughout the rf pulse, the latter being operationally essential at high power.

Electron Heating

The electron temperature increase is maintained for a given rf power level for much longer than was previously the case. The electron temperature measurements shown were obtained from soft X-ray measurements on axis and at r = ± 5.3 cm, normalised to agree with the electron temperature profiles obtained with a single pulse ruby laser Thomson scattering system. We obtain for this shot a peak electron temperature increase of ~150 eV from an initial value of 635 eV, at a line-averaged electron density of $\bar{n}_e = 2.3 \times 10^{13}$ cm^{-3}. We obtain, over a complete power scan, an incremental heating factor of $\bar{n}_e \Delta T_{eo}/P_{RF} = 3.4 \times 10^{13}$ $eV/cm^3 kW$. The increase in electron temperature remains roughly linear with delivered rf power, up to the

highest powers, when the radiated power loss increases too early for the electron temperature to reach its true peak, as shown in Fig. 3.

From the change in the value of dTe/dt we obtain a heating power $3/2\int n_e \dot{T}_e dV \sim 57$ kW. We have not included the term $3/2\int \dot{n}_e T_e dV$ in the estimate of the heating power since puffing experiments accurately simulating the density waveform obtained with rf heating power also showed an increase in this term while the electron temperature remained relatively constant; this suggests that only the slope of the electron temperature should be taken as an indication of net power input.

The subsequent decrease in the electron temperature, which is slow with respect to $\tau_{Ee} \sim 2$ msec, is fully explained by the increase in the radiated power loss during the rf pulse. This has been demonstrated using a simple evolution code.

Radiation and Impurities

We have made a considerable effort to reduce the radiated power loss by studying different limiter designs and materials, namely carbon, Stainless Steel and TiC coated carbon. In Fig. 4 we show the extreme cases of the large surface area stainless steel limiter (Fe-2) and the small surface area carbon limiter (C-2). We see that the peakedness of the radiated power profile is dramatic in the case of the Fe-2 limiter and just hollow before the rf pulse in the case of the C-2 limiter. For constant conditions of plasma current and density we have been able to reduce the core radiated power loss from 2.6 W/cm^3 to 0.6 W/cm^3 during an 80 kW rf pulse under standard conditions. Vacuum UV spectroscopic measurements have confirmed the decrease in metallic impurities. The radiated power from the plasma core must still be due to heavy metallic impurities and the antennae themselves are the most probable source of such impurities, being only 2 cm from the limiter radius. The vessel wall is at its closest on the inside, being only 3.5 cm from the limiter radius. In the autumn we shall be replacing our present antennae by an improved design. The radiated power increases during the rf pulse and this is due, to a large part,

to the increase in plasma density. The radiated power profile has been simulated from the measured electron density and temperature profiles and modelled impurity profiles, assuming coronal equilibrium, and an example is shown in Fig. 5. Peaked heavy impurity concentrations are required to simulate the measured profiles. The value of $Z_{eff}(r)$ is calculated from these profiles from which we obtain $\langle Z_{eff} \rangle$. The agreement between $\langle Z_{eff} \rangle$ measured and simulated, 2.5 and 2.67 respectively is surprisingly good.

In spite of the increase in the electron temperature, the plasma column resistance has still not decreased, and in fact it still increases during the rf pulse. The amount of this increase, for a given rf power, depends on the resistance of the target plasma. There has been a considerable reduction in column resistance, by a factor of two during the year, following the limiter changes and a more intensive discharge cleaning programme. The decrease in target plasma resistance is mainly due to a broader electron temperature profile obtained with carbon or TiC-coated carbon limiters compared with the metal limiters, rather than a considerable decrease in $\langle Z_{eff} \rangle$. The fractional increase in resistance, at a given rf power, has not, however, shown any indication of further reduction. It increases roughly linearly as the rf power delivered is increased and it is also almost independent of the applied mode-structure (N = 1,2 or 4).

These observations are compatible with an impurity concentration increase proportional to the impurity concentration itself. Light impurity sputtering provides such a mechanism. Using Langmuir probes we have investigated the density and electron temperature in the scrape-off layer (Hofmann et al., 1983). We find that the electron temperature increases from typically 8-10 eV to 15-30 eV during the rf pulse (Fig. 6), an increase which is sufficient to produce enhanced sputtering. At the same time, the plasma potential drops to assume a negative value and the plasma density drops. We consider these effects to be due to the power deposited in the plasma, rather than local antenna phenomena related to the electrostatic potential or rf current, and we still do not intend to add an electrostatic shield to our antennae. The rf will, however, have a direct effect on the sputtering coefficient from the antennae themselves. This is obviously only important

once sputtering is already an important mechanism. Fast video films taken under a wide range of conditions have shown no local antenna-related emission in the visible region. Measurements of the scrape-off layer and surface erosion were also performed using surface interaction probes, and in general indicate an increase in the sputtering yield during the rf pulse by as much as a factor of 2-4.

Ion Heating

The ion temperature increase has also been systematically studied. Previously the ion temperature decreased from its maximum level towards the end of the rf pulse. This we associate with the drop in plasma current during those experiments and the increase is now maintained throughout the rf pulse. Under standard conditions, the central ion temperature increases from $T_{io} \sim 250$ eV to ~ 430 eV with 140 kW of rf power and we still find a heating factor value of $\bar{n}_e \Delta T_{io}/Prf = 1.5 \times 10^{13}$ eV/cm^{3}kW under the standard conditions. In hydrogen, and under similar imposed conditions, we obtain a similar figure, namely 1.7×10^{13} eV/cm^{3}kW, with no line-averaged density increase. The increase in ion temperature and the change in dT_{io}/dt at the start of the rf pulse are observed to be linear as a function of delivered rf power as shown in Fig. 3. A part of the ion temperature increase can be due to the increase in density observed at high power. We have studied the ion temperature behaviour in shots during which the density increase is negligible, obtained at modest rf power by closing the gas feed valve before the rf pulse, and we still find a similar increase. We also show in Fig. 7 the locus of T_i vs $\bar{n}_e$, both in a discharge with the rf pulse applied, and with a programmed density increase. We see that with the rf power the ion temperature increases considerably more. We therefore maintain our claim that there is a direct power transfer to the ions. We estimate the power input to the ions from the rate of increase of the ion temperature at the start of the rf pulse; again we neglect $\dot{\bar{n}}_e$ contributions to the power balance for the standard conditions ($\bar{n}_e \sim 2.3 \times 10^{13}$ cm^{-3}, $I_p \sim 123$ kA, D_2, 15 kG) and we obtain $P_i \sim 7.6$ kW. The clearness of the ion heating signal is due to the small electron-ion collisional power transfer, in this case ~ 11 kW integrated out to $r/a \sim 3/4$.

The dissipative mechanism which leads to the ion heating has not been established. It has, however, withstood the changes in limiter material and the corresponding large decrease in the metallic impurity level at the plasma centre.

Density increase

We now turn to the observed plasma density increase. The initial higher power experiments showed a large increase in line-averaged density during the rf pulse. This increase was reduced by better conditioning but has since resisted further modification. Current control has led, in general, to a more definite and continued density ramping rate rather than a simple density increase. The ramping persists at high power, albeit reduced, when the gas feed is completely cut just before the rf pulse. We attribute the previously observed "saturated" increase to a drop in particle confinement and/or recycling rate as the plasma current decreased. The density increase is again relatively insensitive to the applied mode structure (both N and M) under fixed conditions, and its magnitude increases roughly linearly with the rf power. The density increase is, however, dependent on the target plasma density, being considerably smaller relatively and absolutely at higher densities. This behaviour is shown in Fig. 8. We also observe an increase in the density profile peaking factor K_n [$n_e(r) = n_{eo} \times (1-r^2/a^2)^{Kn}$] measured with an 8-channel FIR interferometer. The value of K_n does, however, itself increase with increasing density without the rf pulse. Combined with the observed linear increase in line-averaged density with increasing rf power, the increased peaking factor shows that the peak electron density is increasing faster than linearly. This further exacerbates the problem of enhanced radiated power loss from the plasma core.

Effect of mode structure

The increase in the line-averaged density during the rf pulse serves, in addition, to confuse the interpretation of the effects of the Alfvén Wave mode structure, since the Alfvén Wave spectrum is

swept through during the pulse. We have, as mentioned, observed little correlation between macroscopic parameters and either the excitation structure or the position in the Alfvén Wave spectrum. One striking exception is found at the estimated threshold of the n = 2, m = 0 continuum. Here we find a loading resonance which is assumed to be the (n,m) = (2,0) DAW excited, via toroidal coupling, by the (N,M) = (2,1) antenna structure. In fact, direct excitation using the (N,M) = (2,0) antenna structure shows little loading by this resonance, presumably since there is no (n,m) = (2,0) surface wave at this frequency. The excitation of this DAW is also more pronounced at lower values of q_a when, with a broader current profile, toroidal coupling could be more important. We see in Fig. 9 that at the moment we cross into the (n,m)=(2,0) continuum we observe a maximum in the soft X-ray emission, a break in the density rise, an increase in the D_α emission and a break in the radiated power signal in spite of an increase in delivered rf power. There are also indications that crossing into the (n,m) = (-2,-1) continuum, at a higher density, has a similar effect in reducing the density increase. A weakness of our present antenna system is its inability to excite waves of specified helicity. This weakness has, however, led to the main advances in our understanding of the Alfvén Wave spectrum.

Particle Confinement

We observe a decrease in the line-integrated D_α emission during the rf pulse, in standard conditions, both with and without density feedback. At the same time there is an increase in the height of the wings of the radial profile of the D_α emission, indicative of a change in the electron temperature and density profiles at the plasma edge, and/or a change in the recycling conditions (reflected energy spectrum). The drop in D_α emission together with the increasing plasma density strongly suggests an increase in particle confinement time during the rf pulse. Impurity ionization is rejected as the prime cause of the density increase since the magnitude of the effect has remained similar for very different impurity conditions with the various limiter materials. In addition the effect of the (n,m) = (2,0)

continuum on the density rise demonstrates that the increase in particle confinement during the rf pulse may well be related to the form of the wave-function within the plasma, rather than simply to the power input.

Power Limits

Up to now we have not been able to deliver the maximum available rf power to the plasma although the limiter changes led to substantial improvements, as did improvements to the Tokamak operation. Ramping the rf power up over 10 msec was found to be important in avoiding a disruption early in the rf pulse at high power. Time also plays a role, with improvements in plasma performance continuing over the weeks following a torus opening. It appears evident that the conditioning of new carbon limiters takes several weeks before full rf power can be applied.

Under any condition, however, we find a power level at which the sawtooth activity cannot be maintained during the full duration of the rf pulse. At this power the discharge converts to a mode-dominated regime (MD) which often, especially at high power, leads to a disruption within 5-10 msec. This MD regime is characterized by large amplitude Mirnov oscillations, synchronous with internal soft X-ray flux modulations which occur at the q=1 surface. This mode-locked activity leads, in general, to an increase in the plasma column resistance, an increase in the D_α emission and its fluctuation level, a reduction in the density rise and an increase in the bolometer signal. The sawtooth activity, of course, ceases. When the value of q at the limiter is not far from rational subsequent disruption is likely. When the value of q lies in a relatively small region $3.1 < q_I < 3.5$ then a high level of mode-locked activity can be maintained non-fatally, provided the plasma position is slightly to the outside.

The choice of the carbon limiter for present operation was made on its ability to promote sawtooth dominated discharges (SD) although the TiC-coated graphite limiters provided a lower ratio of P_{rad}/P_{oh}. We assume that the more hollow radiated power profile in

the case of the carbon limiters is important, or, in other words, that the high radiated power on axis is the main trigger of MD discharges, hence of our observed power limits.

In addition, SD discharges at the highest powers can also disrupt without apparently having converted to prolonged, q-related MD activity. This occurs late in the rf pulse, when the density, radiated power and plasma resistance have reached abnormally high values, is preceded by a short burst of mode-locked activity, and is obviously related to the observed accumulation of heavy impurities at the plasma centre.

CONCLUSIONS

Following limiter changes and operational improvements we have succeeded in delivering rf power up to 206 kW, roughly equal to the ohmic power, into standard discharges.

Both electron and ion heating are observed with a measured total heating factor of $\bar{n}_e(\Delta T_{eo}+\Delta T_{io})/P_{rf} = 4.9\times10^{13}$ eV/cm^{3}kW.

We find an increase in both electron density and radiated power loss which limit the power we can deliver without suffering a major disruption.

We have related the impurity problem to changes in the scrape-off layer, measured using Langmuir probes.

We have found first evidence of an increase in particle confinement during the rf pulse and it is related to the Alfvén wave spectrum excited.

ACKNOWLEDGEMENTS

We thank MM. M. Grossmann, Ph. Marmillod, A. Tuszel and the TCA support team for their continued endeavour. The stimulation and encouragement received from Prof. F. Troyon must also be recognized. The work in this paper was partly supported by the Swiss National Science Foundation.

REFERENCES

Appert, K., R. Gruber, F. Troyon, and J. Vaclavik (1982). Plasma Physics, 24, 1147-1159.

Bengtson, R.D., J.F. Benesch, T.E. Evans, Y.-M. Li, S.M. Mahajan, R.B. Michie, M.E. Oakes, D.W. Ross, P.M. Valanju, X.-Z. Wang, and J.G. Watkins (1983). 5th Topical Conf. on RF Heating in Plasmas, Wisconsin.

Cheetham, A.D., A. Heym, F. Hofmann, K. Hruska, R. Keller, A. Lietti, J.B. Lister, A. Pochelon, H. Ripper, A. Simik, and A. Tuszel (1980). Proceedings 11th Symp. on Fusion Technology, Oxford.

De Chambrier A., A.D. Cheetham, A. Heym, F. Hofmann, B. Joye, R. Keller, A. Lietti, J.B. Lister, and A. Pochelon (1982a). Plasma Physics 24, 893-902.

De Chambrier A., A.D. Cheetham, A. Heym, F. Hofmann, B. Joye, R. Keller, A. Lietti, J.B. Lister, A. Pochelon, W. Simm, J.L. Toninato, and A. Tuszel (1982b). Proceedings 9th Int. Conf. on Plasma Physics and Contr. Nucl.Fusion, Baltimore.

Cross, R.C., B.D. Blackwell, J.A. Lehane, G. Borg, and M.H. Brennan (1982. Proceedings 3rd Joint Varenna-Grenoble Int. Symp. Vol. I, 183 EUR7979EN.

Demirkhanov R.A., A.G. Kirov, G.I. Astapenko, S.E.Il'Inskij, E.M. Lomakin, V.V. Onishchenko, L.F. Ruchko, A.V. Sukachev, V.D. Medun, and N.I. Malykh (1982). Proceedings 9th Int. Conf. on Plasma Physics and Contr. Nucl.Fusion, Baltimore.

Hasegawa A. and C. Uberoi (1982). "The Alfvén Wave", U.S. DOE.

Hofmann F., Ch. Hollenstein, B. Joye, A. Lietti, J.B. Lister and A. Pochelon (1983). Accepted for publication by J. Nuclear Materials.

Prager S.C., F.D. Witherspoon, C.E. Kieras, D. Kortbawi, J.C. Sprott, and J.A. Tataronis (1983). 5th Topical Conf. on RF Heating in Plasmas, Wisconsin.

FIGURE CAPTIONS

1. Antenna Loading as a function of density (15 kG, D_2, 2.5 MHz)
   a) Experimental curves
   b) Theoretical calculation

2. Waveforms for typical discharge (15 kG, D_2).

3. Variation of parameters as a function of peak delivered rf power.

4. Radiated power profiles
   a) Wide stainless-steel limiters
   b) Narrow graphite limiters

5. Modelled radial profile of Z_{eff}.

6. Scrape-off layer measurements (15 kG, D_2, $q = 4.3$)

7. Focus of T_i vs $\bar{n}_e$ with and without rf.

8. Behaviour of the density increase during the rf pulse.

9. Effect of the (2,0) continuum threshold on the density rise.

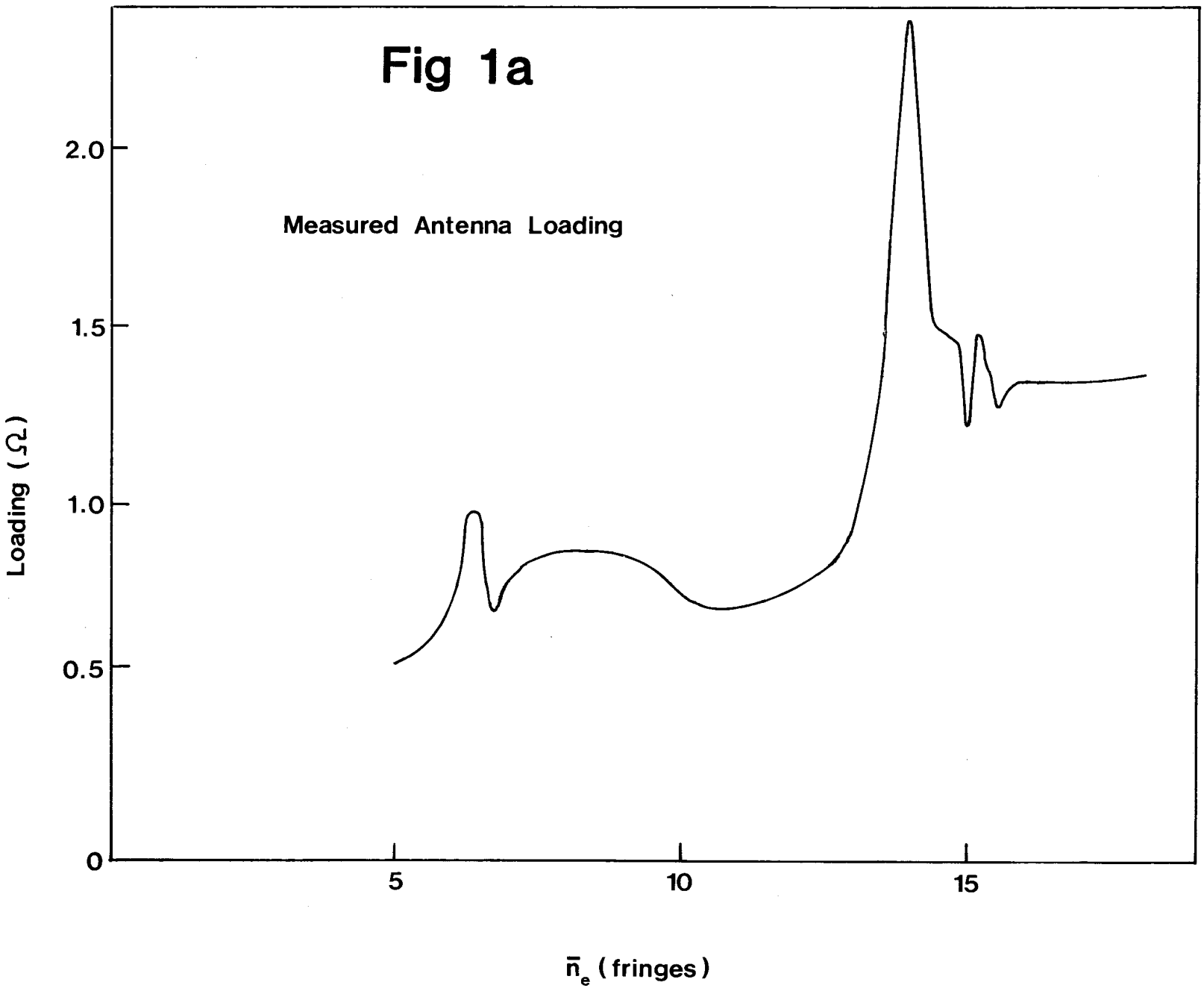
Fig 1a
Measured Antenna Loading
2.0
1.5
1.0
0.5
0
Loading (Ω)
5
10
15
$\bar{n}_e$ (fringes)

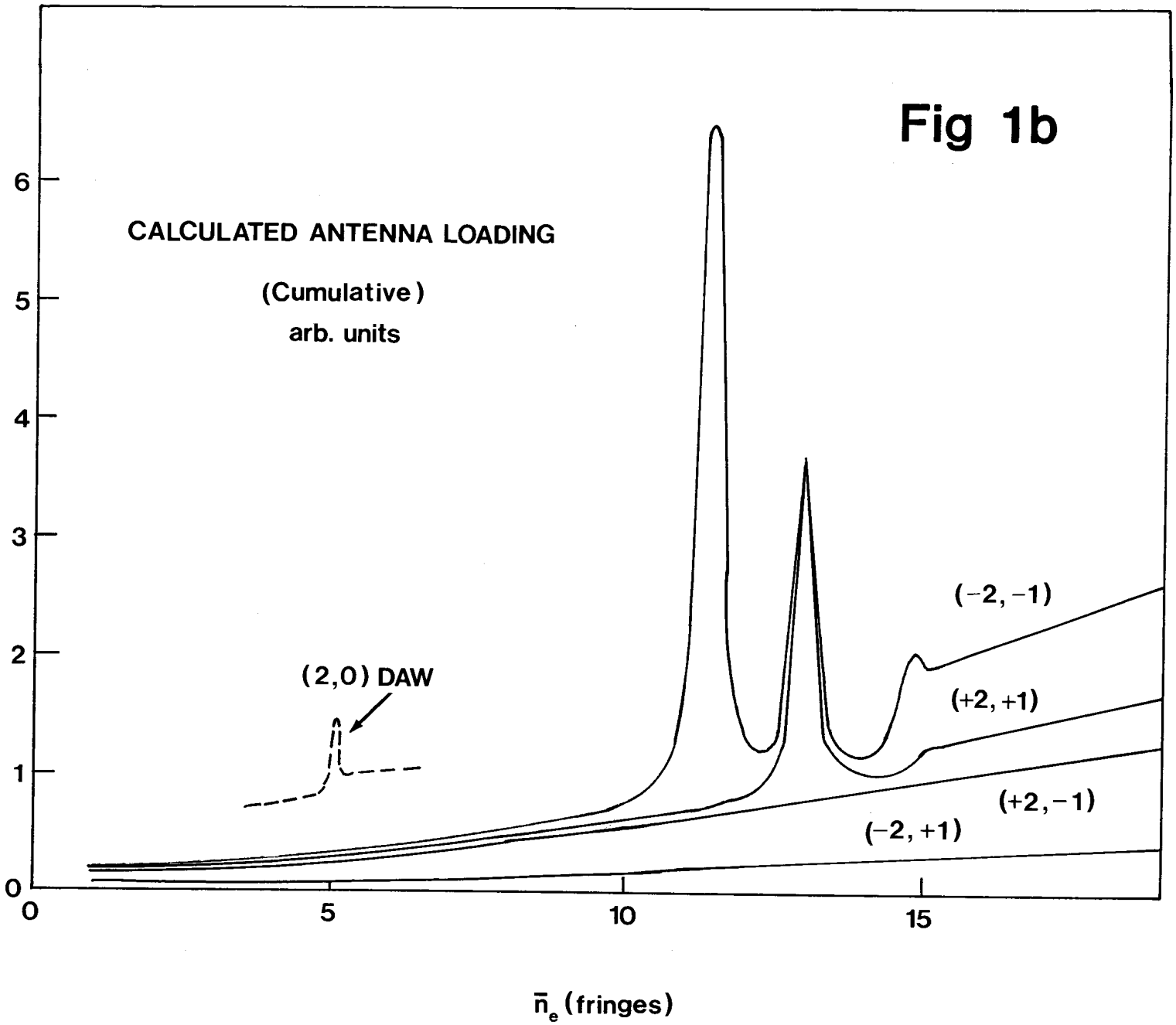
Fig 1b
CALCULATED ANTENNA LOADING
(Cumulative)
arb. units
6
5
4
3
2
1
0
0
5
10
15
(2,0) DAW
(−2, −1)
(+2, +1)
(+2, −1)
(−2, +1)
$\bar{n}_e$ (fringes)

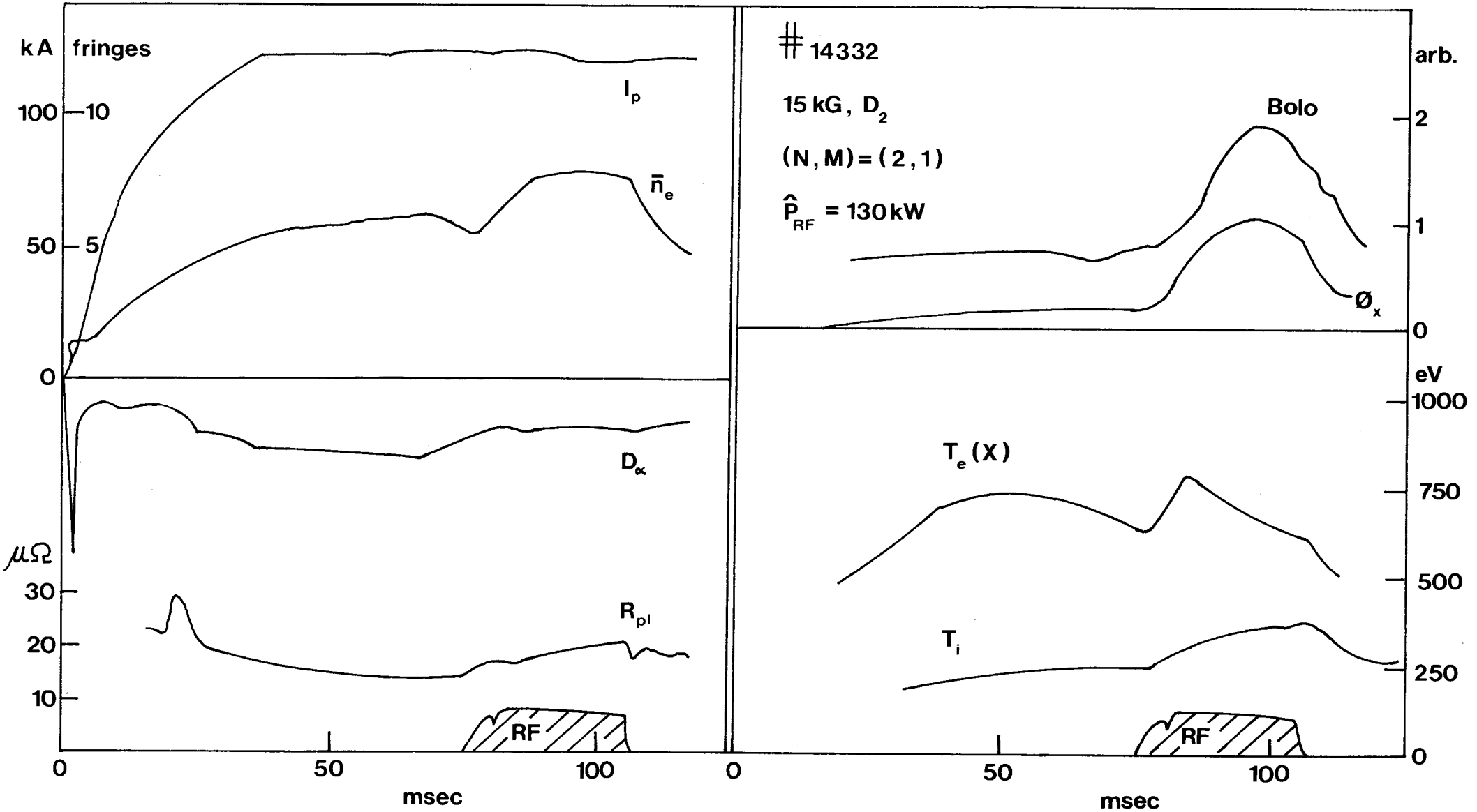
kA
fringes
100
10
50
5
0
I_p
$\bar{n}_e$
D_α
μΩ
30
20
10
R_{pl}
RF
0
50
100
msec
#14332
15 kG, D_2
$(N, M) = (2, 1)$
$\hat{P}_{RF}$ = 130 kW
arb.
2
1
0
Bolo
$\emptyset_x$
eV
1000
750
500
250
0
$T_e(X)$
T_i
RF
0
50
100
msec

Fig 2

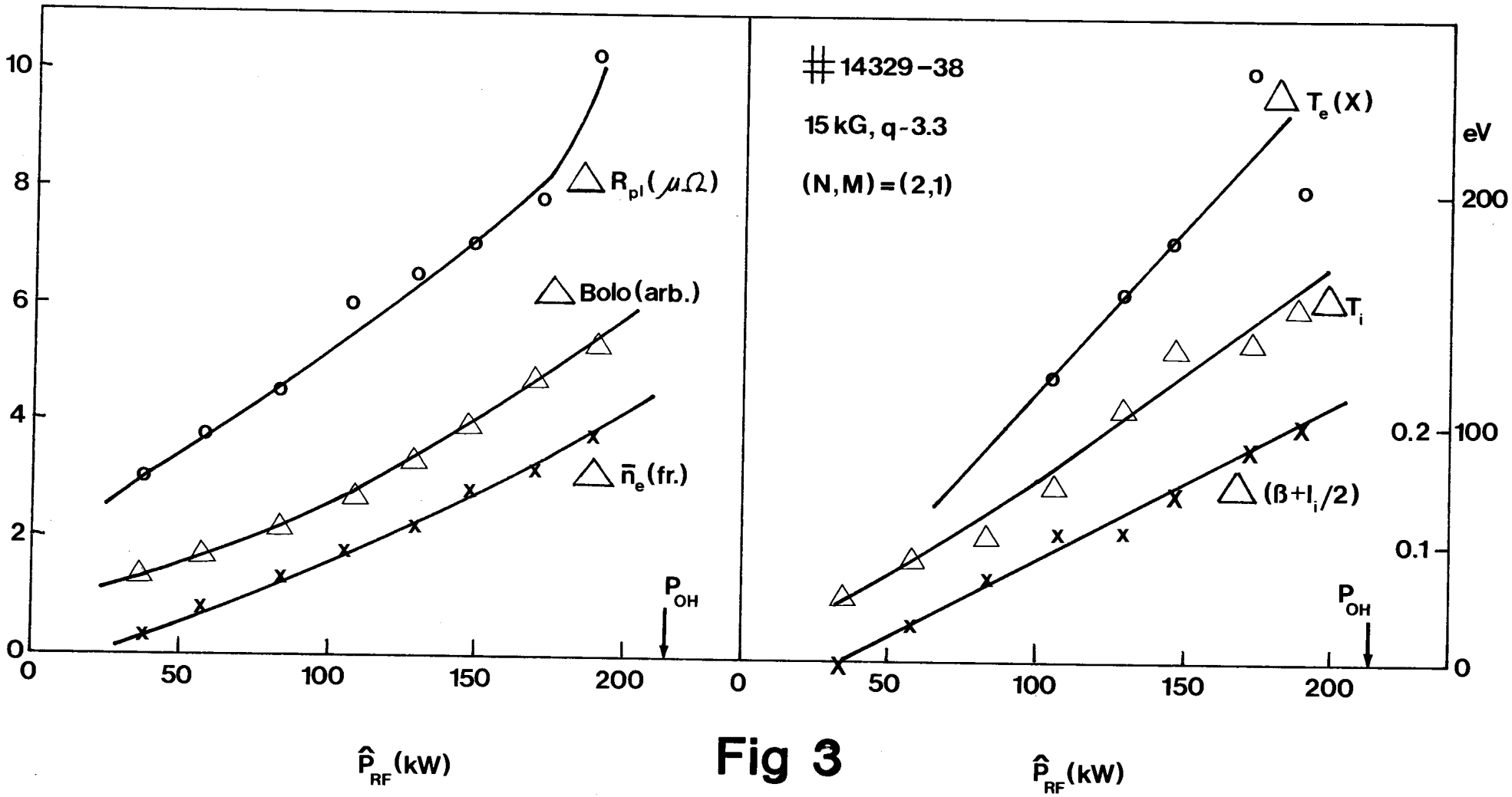
10
8
6
4
2
0
0
50
100
150
200
$R_{pl}(\mu\Omega)$
Bolo (arb.)
$\bar{n}_e$(fr.)
P_{OH}
$\hat{P}_{RF}$(kW)
#14329-38
15 kG, q-3.3
(N,M) = (2,1)
T_e(X)
T_i
$(\beta+l_i/2)$
eV
200
100
0
0.2
0.1
0
50
100
150
200
P_{OH}
$\hat{P}_{RF}$(kW)

Fig 3

Fig 4a

Fe–2

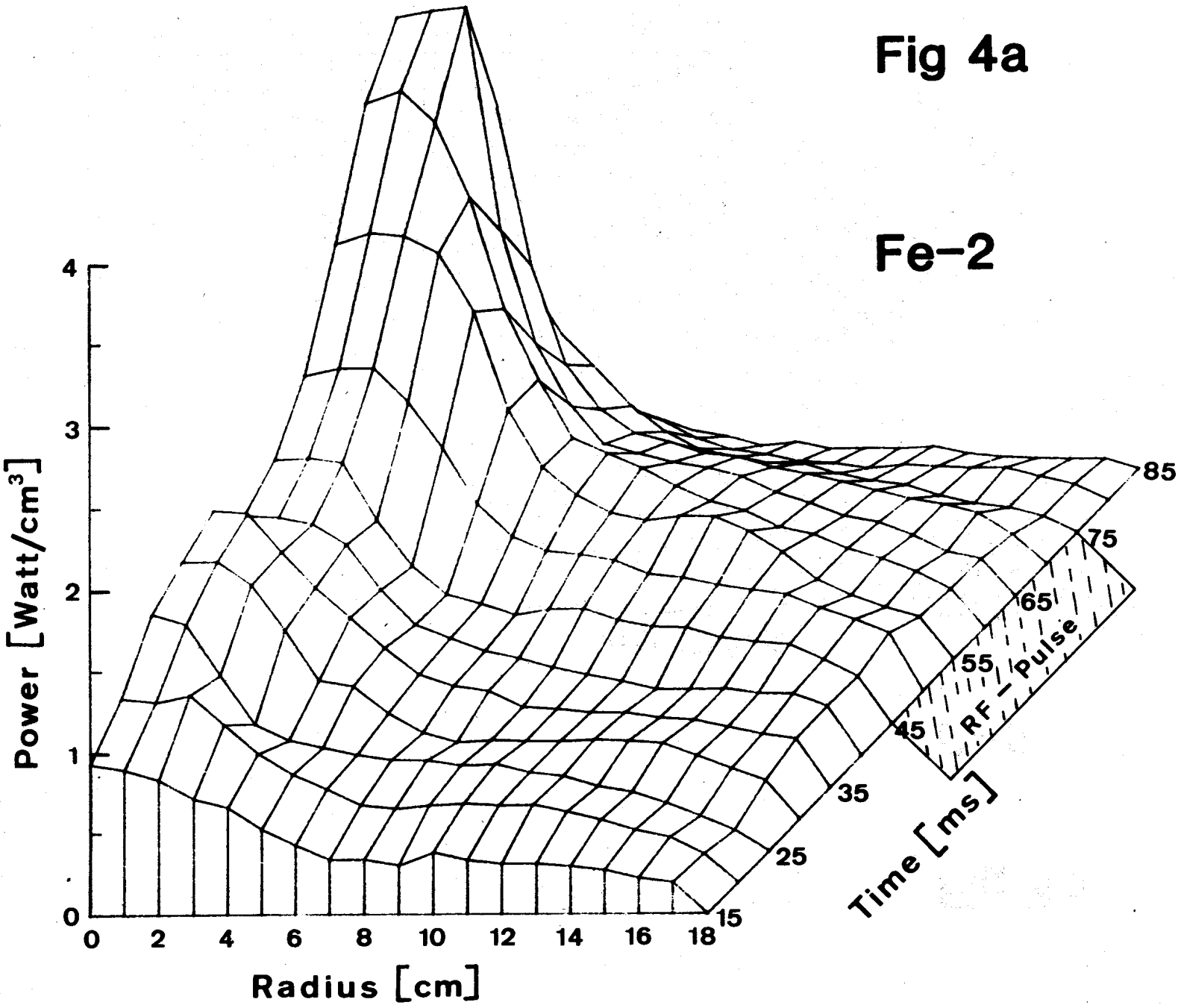
Power [Watt/cm³]
4
3
2
1
0
0
2
4
6
8
10
12
14
16
18
Radius [cm]
15
25
35
45
55
65
75
85
RF – Pulse
Time [ms]

Fig 4b

C-2

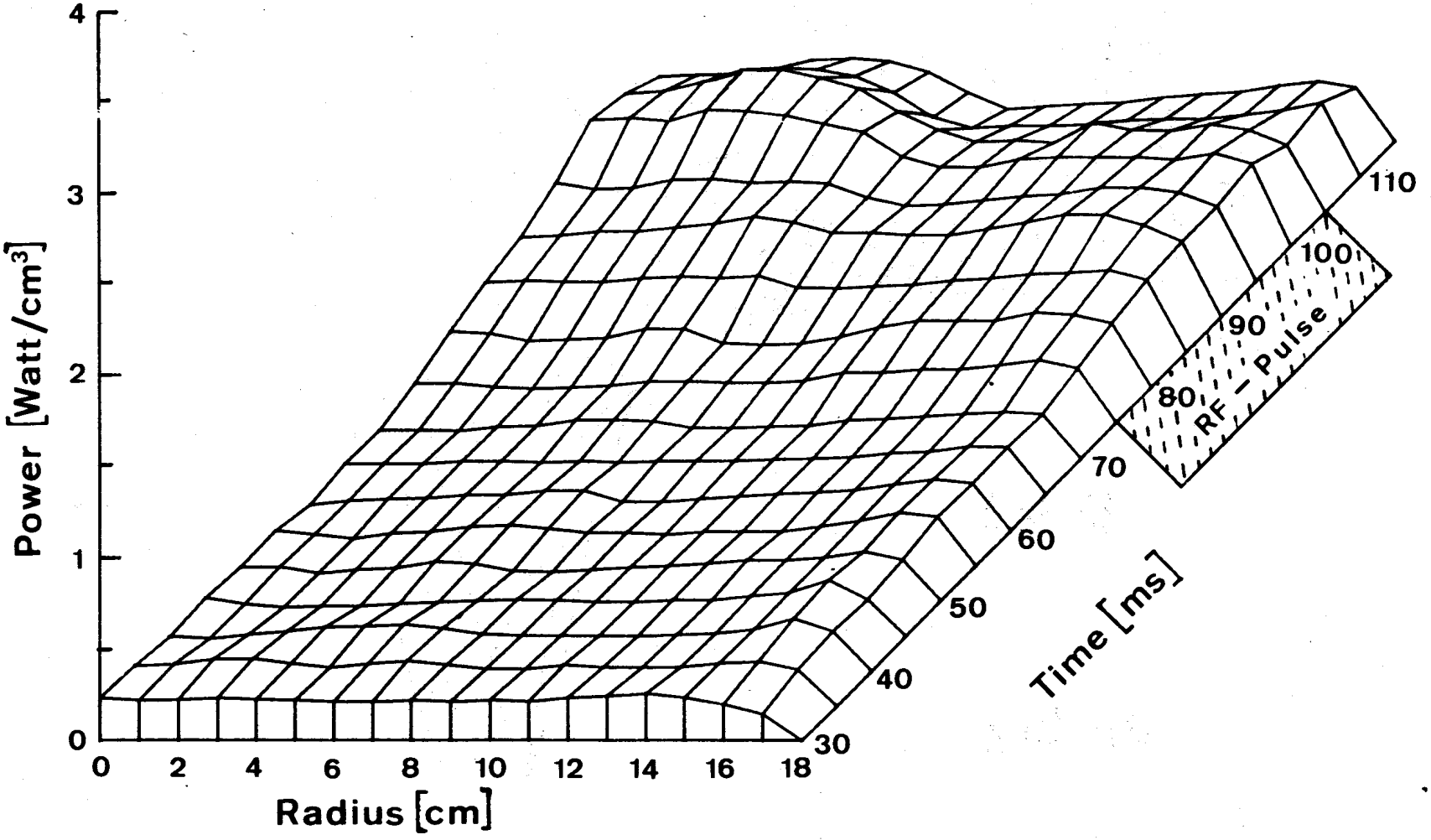
Power [Watt/cm³]
0
1
2
3
4
0 2 4 6 8 10 12 14 16 18
Radius [cm]
30
40
50
60
70
80
90
100
110
RF - Pulse
Time [ms]

Fig 5

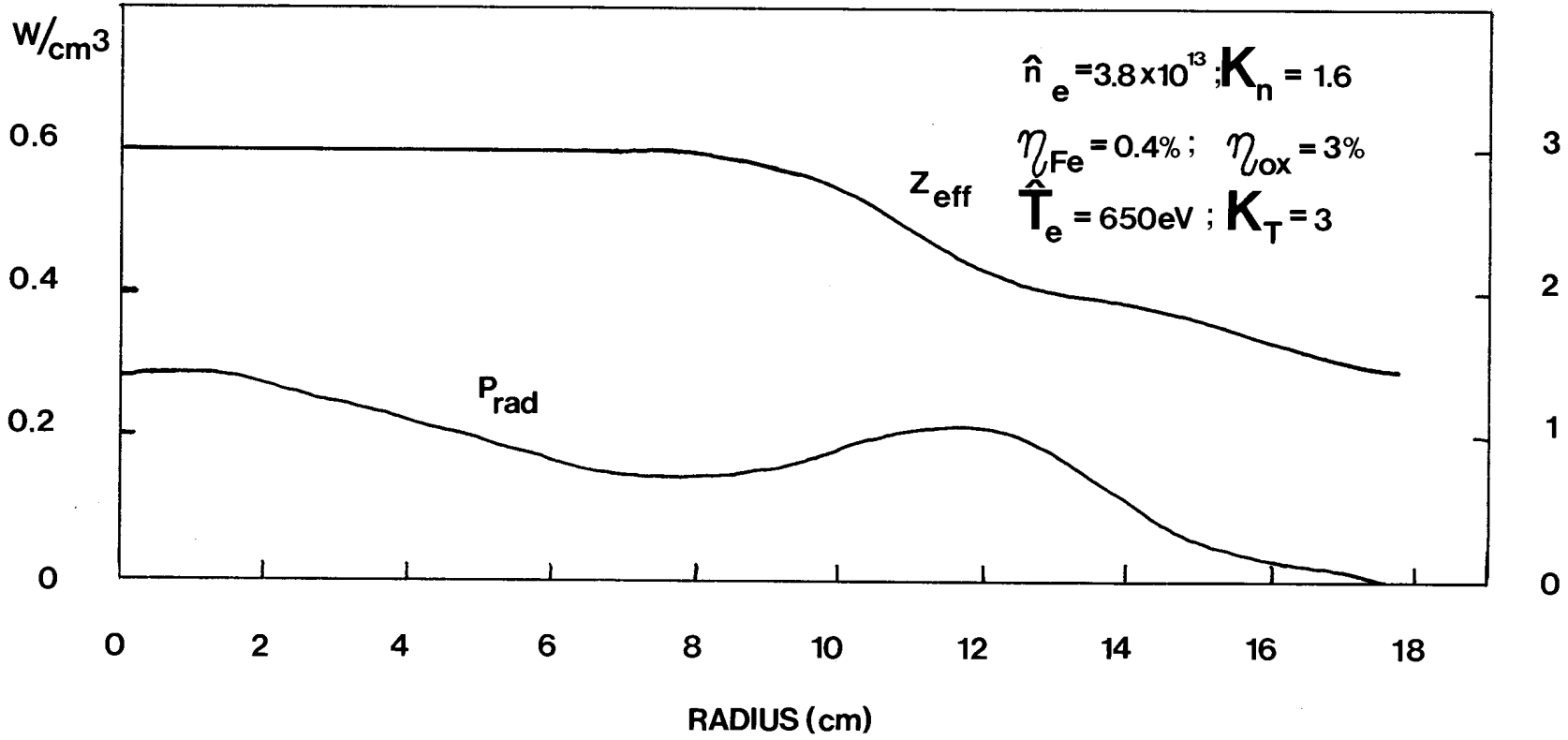
W/cm3
0.6
0.4
0.2
0
3
2
1
0
$\hat{n}_e = 3.8 \times 10^{13}$; $K_n = 1.6$
$\eta_{Fe} = 0.4\%$; $\eta_{ox} = 3\%$
$\hat{T}_e = 650eV$; $K_T = 3$
Z_{eff}
P_{rad}
0
2
4
6
8
10
12
14
16
18
RADIUS (cm)

Fig 6

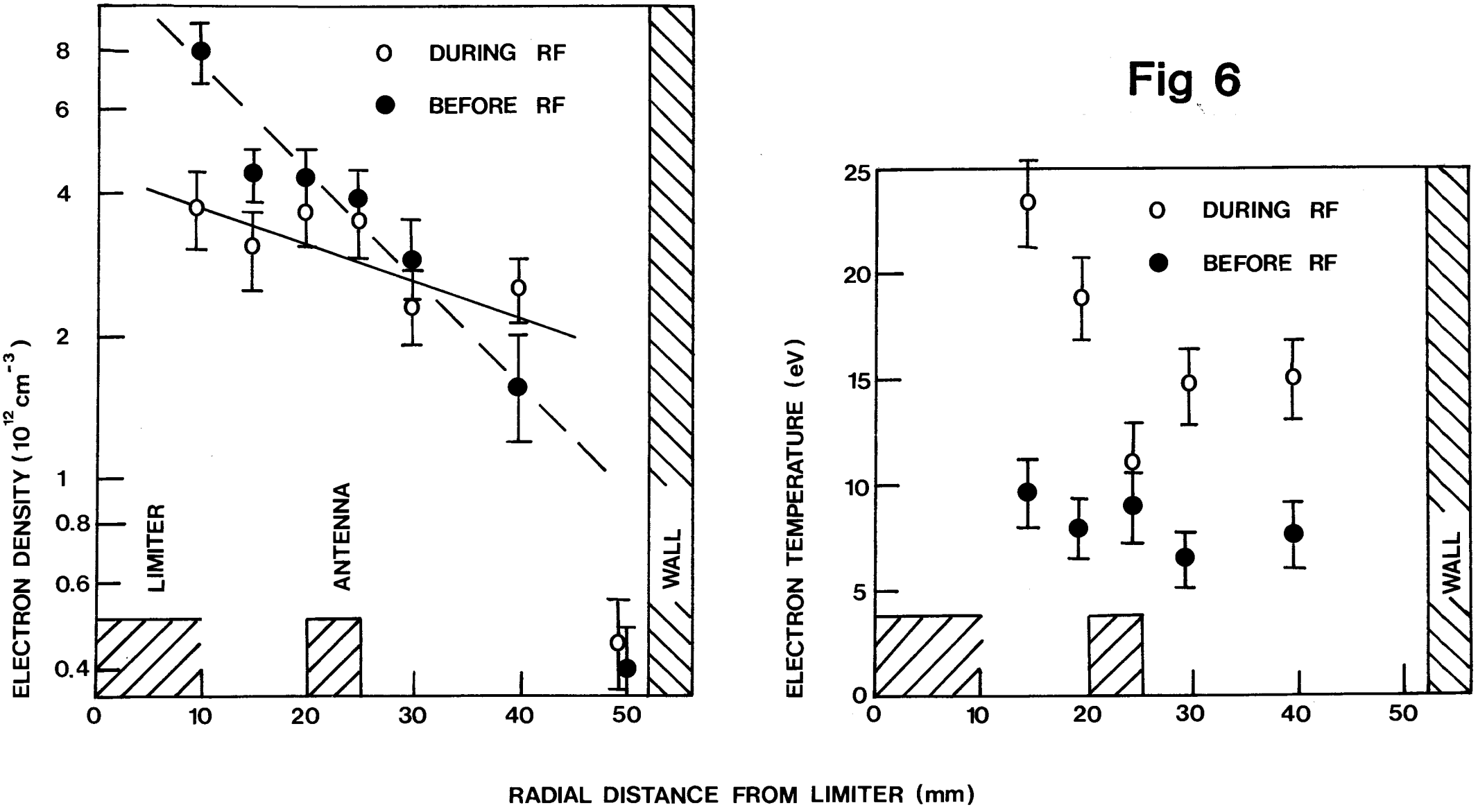
O DURING RF
● BEFORE RF
ELECTRON DENSITY (10^{12} cm^{-3})
8
6
4
2
1
0.8
0.6
0.4
LIMITER
ANTENNA
WALL
0
10
20
30
40
50
ELECTRON TEMPERATURE (eV)
25
20
15
10
5
0
RADIAL DISTANCE FROM LIMITER (mm)

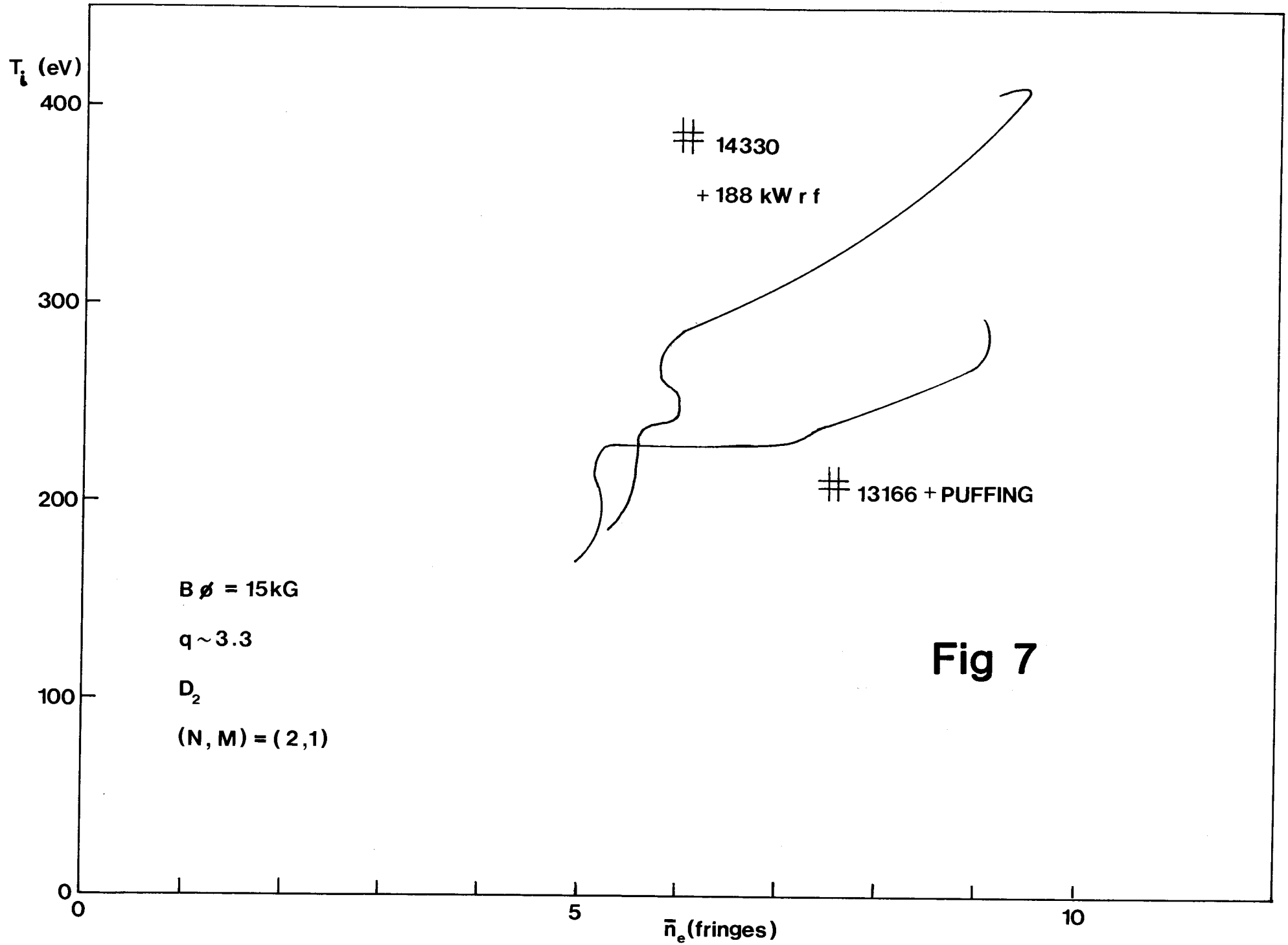
T_i (eV)
400
300
200
100
0
0
5
10
$\bar{n}_e$(fringes)
14330
+ 188 kW r f
# 13166 + PUFFING
B ø = 15kG
q ~ 3.3
D_2
(N, M) = (2,1)

Fig 7

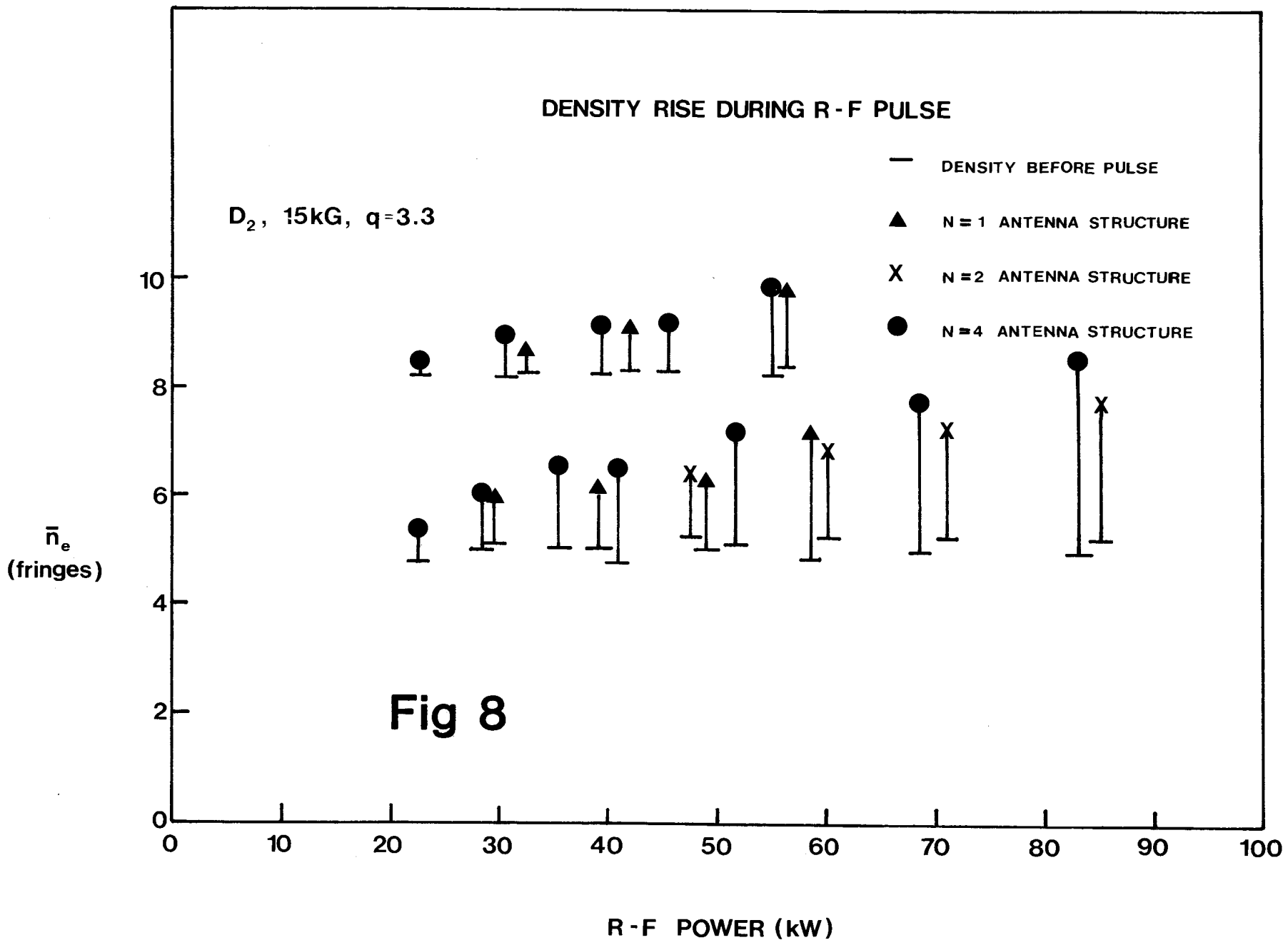
DENSITY RISE DURING R-F PULSE
D_2, 15kG, q=3.3
DENSITY BEFORE PULSE
N = 1 ANTENNA STRUCTURE
N = 2 ANTENNA STRUCTURE
N = 4 ANTENNA STRUCTURE
$\bar{n}_e$ (fringes)
0
2
4
6
8
10
0
10
20
30
40
50
60
70
80
90
100
R-F POWER (kW)

Fig 8

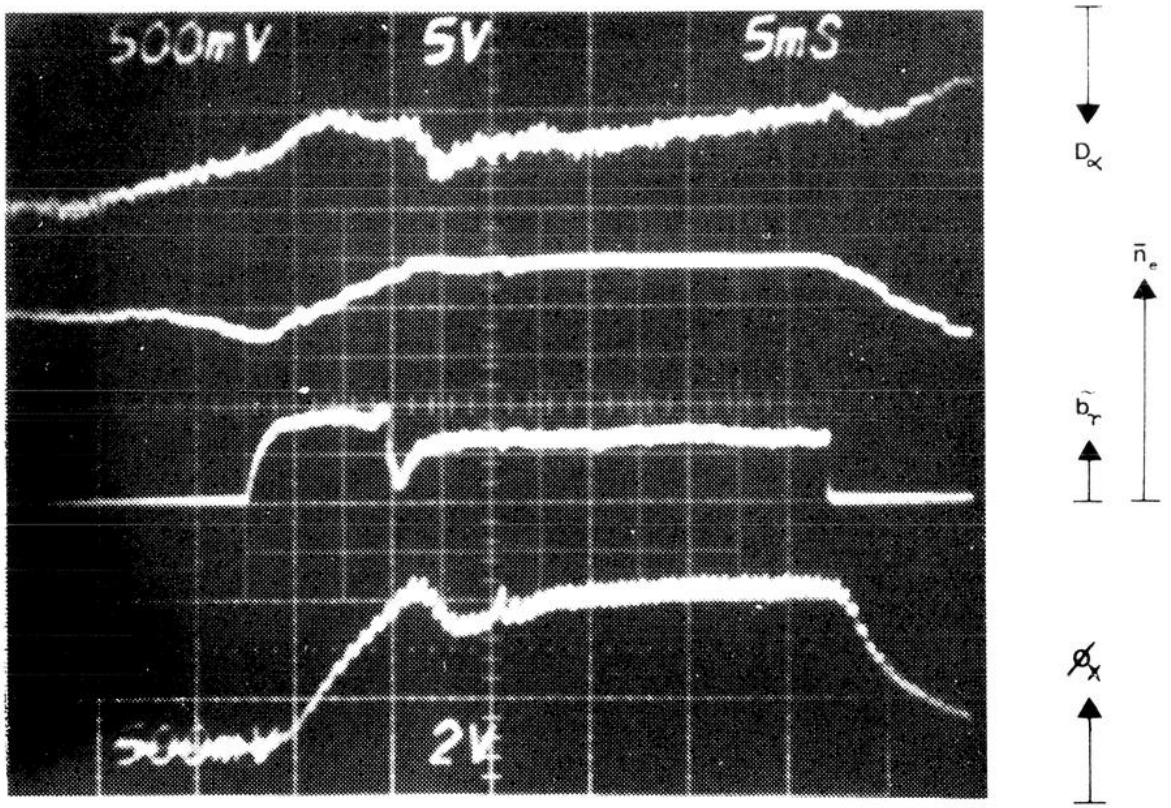

Fig 9